Materials Science & Engineering A 582 (2013) 305–315

Contents lists available at SciVerse ScienceDirect

Materials Science & Engineering A

journal homepage: www.elsevier.com/locate/msea

Toughening mechanism for Ni–Cr–B–Si–C laser deposited coatings

I. Hemmati, V. Ocelík *, J.Th.M. De Hosson

Materials innovation institute (M2i), Department of Applied Physics, University of Groningen, Nijenborgh 4, 9474 AG Groningen, The Netherlands

ARTICLE INFO

Article history:
Received 8 March 2013
Received in revised form
30 May 2013
Accepted 1 June 2013
Available online 15 June 2013

Keywords:
Ni-base hardfacing alloys
Laser deposition
Cracking
Microstructural refinement

ABSTRACT

Laser deposited coatings were made from Colmonoy 69 Ni–Cr–B–Si–C alloy and Nb-modified Colmonoy 69 using laser cladding with powder injection. Addition of Nb was done to decrease the structural scale of Cr boride precipitates by providing Nb-rich nucleation agents. The purpose of the study was to evaluate the viability of microstructural refinement as a toughening mechanism for Ni–Cr–B–Si–C alloys. The results show that although a significant refinement of the Cr-rich precipitates while preserving the original level of hardness could be induced in these alloys by a suitable addition of Nb, cracking susceptibility of the deposits was not decreased. This is attributed to the continuous network of hard eutectics providing an easy route for crack growth. The outcome of this work points out that an effective toughening mechanism for Ni–Cr–B–Si–C alloys should include not only refinement of the hard precipitates, but also modification of the eutectic structure.

1. Introduction

Ni–Cr–B–Si–C hardfacing alloys are among the most widely used alloys for applications requiring corrosion and wear resistance. These alloys with their low melting point (e.g. solidus temperature of 940 °C according to manufacturer's datasheet for Colmonoy 69 alloy studied in this work) and self-fluxing properties were originally developed for spray and fuse applications. However, in recent years, laser deposition technologies were successfully used to produce dense Ni–Cr–B–Si–C coatings with metallurgical bonding to the substrate and superior functional properties [1–3]. Despite the desirable corrosion and wear properties of Ni–Cr–B–Si–C alloys and their potential for many surface coating, repair and free-form manufacturing applications [4–6], high cracking propensity poses a serious drawback to their usage in laser deposition technologies [7].

Considerable efforts have been made to solve the cracking problem of laser deposited Ni–Cr–B–Si–C alloys either by reducing the tensile stresses in the clad layers via preheating and controlled cooling [4,8–10] or by increasing the ductility of these alloys through modification of their phase constitution and microstructure [7,10–12]. The latter approach is more attractive from practical and economic viewpoints, especially for large area depositions. Lowering the alloy content of Ni–Cr–B–Si–C alloys, e.g. B or Cr content, will improve their toughness but at the expense of some hardness [13]. As Ni–Cr–B–Si–C alloys are mostly intended for wear applications, solving the cracking problem by lowering their high hardness and deteriorating their wear resistance is not a preferable solution. Consequently, studies have been done in the past to toughen these alloys not by depleting them out of elements such as B and Cr, but by refining their microstructure or eliminating the large brittle Cr-rich precipitates.

The microstructural refinement as a toughening mechanism for laser-deposited Ni–Cr–B–Si–C alloys is based on the idea that the main reason for poor toughness of these alloys [13] is the presence of large Cr boride and carbide precipitates which act as sites for crack nucleation as well as easy routes for crack growth [7,14]. Cr-rich precipitates such as CrB, Cr_5B_3 or Cr_7C_3 [15] are hard and brittle phases which can easily fracture under the rapid cooling rates associated with laser deposition ($\sim 10^3$ K/s [16]) as also confirmed by microstructural observation of crack growth path in these alloys [10]. The stress concentration at the tip of an individual fractured Cr-rich precipitate will determine the probability of crack propagation. The maximum stress σ_m at the crack tip in a brittle phase is directly proportional to the crack length, and can be described as [17]

$$\sigma_m = 2\sigma_a\sqrt{\frac{a}{2\rho_c}} \quad (1)$$

where σ_a is the applied stress, ρ_c radius of curvature for crack tip and a length of the crack, i.e. size of the precipitate. Given the active contribution of Cr-rich precipitates to the cracking phenomena [10], it is expected to observe improvements in cracking susceptibility of the deposits with refined precipitates, i.e. smaller a.

Different alloying elements have been previously added to Ni–Cr–B–Si–C alloys to either prevent formation of Cr borides/carbides (e.g. by addition of tantalum [12] or titanium [11]) or reduce their

* Corresponding author. Fax: +31 50 363 4881.
E-mail address: v.ocelik@rug.nl (V. Ocelík).

0921-5093/$ - see front matter © 2013 Elsevier B.V. All rights reserved.
http://dx.doi.org/10.1016/j.msea.2013.06.010

size by producing new phases which can act as nucleation sites (e.g. by addition of vanadium [7,10]). There have been claims of improvements in toughness of the modified deposits [7,11,12]. However, the cracking problem of these alloys especially while keeping their high level of hardness has not been solved yet.

As mentioned before, Ni–Cr–B–Si–C alloys are mostly intended for wear applications. Hence, a toughening mechanism for these alloys will be most favorable if it is not accompanied by a significant loss of hardness. Such an approach in which enhancement of fracture toughness occurs while preserving the high hardness of the deposits has been successfully tested for Fe-based wear resistant alloys [18,19]. In that case, the key to obtaining a favorable combination of high hardness and high fracture toughness was refinement of the borocarbide precipitates. Based on these analyses, it seems that microstructural refinement may also be a viable toughening mechanism for Ni–Cr–B–Si–C alloys.

A true microstructural refinement of these alloys has not been proven to occur for the previous compositional modifications, mainly because of inaccurate selection of the refining element. A number of rules were proposed in our previous work for selection of a refining element suitable for this alloy system [10]. These rules can be summarized as follows:

(i) Affinity of the refining element for B or C should be higher than affinity of Cr for these elements. In other words, the refining element should have the possibility of preferential formation of borides or carbides during solidification.
(ii) The boride or carbide precipitates of the refining element should have a limited solid solubility in their Cr-rich counterparts.
(iii) The boride or carbide precipitates of the refining element should form at a higher temperature in comparison to Cr-rich precipitates.

The use of these rules can be demonstrated by explaining the lack of microstructural refinement in the vanadium modified Ni–Cr–B–Si–C alloys [10]. Vanadium-rich precipitates either have a complete solid solubility in their Cr-rich counterpart (VB and CrB have complete mutual solubility) or form at low temperatures (as is the case for VC). Addition of vanadium produced new phases and induced morphological changes in the phases of the original Ni–Cr–B–Si–C alloy. But as the second and third rules above were not fulfilled, no considerable refinement was generated by vanadium addition [10].

Analysis of the early transition metals, using the above-mentioned rules in order to find a suitable candidate for the refining element, led us to niobium. Borides and carbides of Nb have large negative values of Gibbs energy of formation [20], have little solubility in Cr-rich phases [21] and form at very high temperatures [22,23]. In this study, a high-alloy grade of Ni–Cr–B–Si–C family was modified with different amounts of Nb addition which resulted in a substantial microstructural refinement as expected while preserving the hardness of original alloy. In this way, it was possible to evaluate the effects of microstructural refinement on cracking tendency of the deposits.

The purpose of this work is two-fold: first, to evaluate the effects of Nb addition on microstructure and properties of a commercial Ni–Cr–B–Si–C alloy with special interest in refining the microstructure of the deposits while preserving their high hardness and second, to assess whether microstructural refinement can function as a viable toughening mechanism for laser deposited Ni–Cr–B–Si–C alloys or not. The outcome of this study enhances our understanding of the microstructure–fracture correlation in this alloy system and may help develop high toughness–high hardness Ni-base wear-resistant alloys.

2. Experimental procedure

Colmonoy 69 (one of the hardest and most brittle Ni–Cr–B–Si–C alloys) was selected as the coating material and for later modifications with Nb. Single and multi-track (5 tracks with 33% overlapping) coatings of Colmonoy 69 and Nb-modified Colmonoy 69 with a thickness of 0.9–1.1 mm were deposited at a speed of 5 mm/s using a side cladding powder injection nozzle, an IPG fiber laser and argon as powder carrier and melt pool shielding gas. A Metco Twin 10C powder feeder was used to simultaneously inject Colmonoy 69 and Nb powders (99.9 wt% purity) to the melt pool. The powders were mixed in a cyclone before exiting the nozzle. Nb powder feeding rates were adjusted to have 2–10 wt% of Nb in the final deposits. S355 carbon steel rods with 50 mm diameter were used as substrate. Chemical compositions of the coating and substrate materials are presented in Table 1. Deposits were made using laser powers of 800–900 W on substrates at room temperature or preheated to 500 °C. Preheating of the substrates was done immediately before cladding using an electric tube furnace and the coated bars were left in the furnace to cool slowly down to the room temperature.

Dilution from the substrate calculated by dividing the surface area of the remelted substrate to the total area of the deposited layer plus remelted substrate [24] evaluated from optical microscopy (OM) images of transversal cross-sections was kept in the range of 5–15% by adjusting the laser power. Samples for OM, scanning electron microscopy (SEM) and hardness measurements were cut and prepared by standard mechanical grinding with suspensions containing 9 and 3 μm diamond particles and polishing with colloidal Al_2O_3. The samples were observed by OM and SEM in the as-polished state. A Philips XL30 Field Emission Gun SEM was used for microstructural observations in Secondary Electron (SE) and Backscattered Electron (BSE) imaging modes. The constituent elements of intended phases were determined by Energy Dispersive Spectroscopy (EDS) mapping and spot analyses using an SUTW+ detector and *EDAX Genesis*® software. To ensure the accuracy and reliability of the EDS measurements, the following steps were taken:

(i) Large precipitates were analyzed to reduce effects of the surrounding matrix.
(ii) An accelerating voltage of 5 kV was used to increase the amount of boron and carbon X-ray signals and maximize the sensitivity of the detector for low-energy X-ray of these elements [25]. EDS maps of the other elements were taken at 20 kV.
(iii) A Standardless Element Coefficient (SEC) of 4 for boron and 2 for carbon were applied in the *EDAX Genesis*® software to compensate for the limited detector accuracy for X-ray lines below 1 keV [15]. A similar approach has been reported to determine the SEC factor for other light elements such as oxygen [26].
(iv) The halographic peak deconvolution (HPD) function in the *EDAX Genesis*® software was used to compare the model EDS spectra with the experimental ones to distinguish the overlap between B–K and Nb–M peaks.

Table 1
Nominal chemical composition of the cladding and substrate materials (wt%).

Material	Ni	Fe	Cr	Si	C	B	Mn	Mo	Cu
Colmonoy 69	Bal.	4	13.5	4	0.7	3	–	2.1	1.7
S355	0.7	Bal.	0.2	0.55	0.12	–	1.65	0.08	0.3

Electron backscatter diffraction (EBSD) patterns were obtained at 30 kV using *TSL OIM Data Collection* and analyzed by *TSL OIM Analysis 5.31* software. A list of possible candidate phases was gathered based on the EDS results. If the structure file for any of the candidate phases did not exist in the *TSL database* (the standard database of the *OIM* software), the structure file had to be created and optimized. For this purpose, the link to the database of *International Center for Diffraction Data* (*ICDD*) was used to generate the structure files for each candidate. Later on, these structure files were optimized by collecting and indexing several high resolution patterns from the intended precipitates. Reflectors were optimized by visual scrutiny and manual adjustments to obtain fit values of less than 1° (the 'fit' parameter in *TSL* softwares which is the angular error between the collected and predicted patterns). Full details on the application of EDS/EBSD for phase identification in this alloy system could be found elsewhere [15].

The crack growth paths and fracture surfaces were studied using both OM and SEM. An attempt was made to measure the toughness of the deposits by indentation at loads of 125, 250, 500, 1000 and 1500 N using the Palmqvist indentation technique [19] which was unsuccessful mainly because of insufficient thickness of the deposits. As a result, the cracking rate was taken as a measure of toughness. The cracking rate was calculated as the number of cracks per unit area of the clad layers by counting the cracks in multi-track samples (deposited on preheated substrates) under a low-magnification ($20\times$) optical microscope. Vickers hardness of the deposits was measured at a load of 4.9 N. Also, Vickers hardness of the eutectic areas in Nb-modified deposits was measured by several single indentations using a force of 0.98 N.

3. Results

3.1. Microstructural effects of Nb addition

Fig. 1 compares a typical microstructure of Colmonoy 69 deposits in (a) with microstructure of the deposits modified by around 4 wt% of Nb shown in (b). According to our previous phase identification study [15], the dark phases in Fig. 1(a) are mainly Cr boride precipitates such as CrB and Cr_5B_3 and the bright background consists of Ni solid solution dendrites and Ni–B–Si eutectics. By comparing Fig. 1(a) and (b), it is clearly visible that addition of Nb significantly refined the microstructure of the deposits, i.e. reduced the size of Cr-rich precipitates. The mechanism of this microstructural refinement was providing the system with many Nb-rich nucleation agents on which the Cr borides were formed (Fig. 1(c)). A true microstructural refinement only happened for specific amounts of Nb addition (in this case, around 4 wt% Nb). Microstructure of the deposits with excessive Nb additions was not refined as shown in Fig. 1(d). The inset of Fig. 1(d) shows that while Nb-rich phases (visible as bright components) still acted as nucleation sites, their size was increased substantially. In addition, large quantities of eutectic phases appeared for higher Nb additions.

Fig. 1(a) shows a *typical* microstructure of Colmonoy 69 deposits. Our previous works showed that this alloy has a tendency to develop multiple microstructures from the same melt chemistry, i.e. similar dilution levels during laser deposition of a fixed alloy powder, with gradual and abrupt changes from one microstructure to another one along the length and depth of the deposits [15,27]. The reason for such a tendency is the large solidification range of Colmonoy 69 alloy and its possibility to

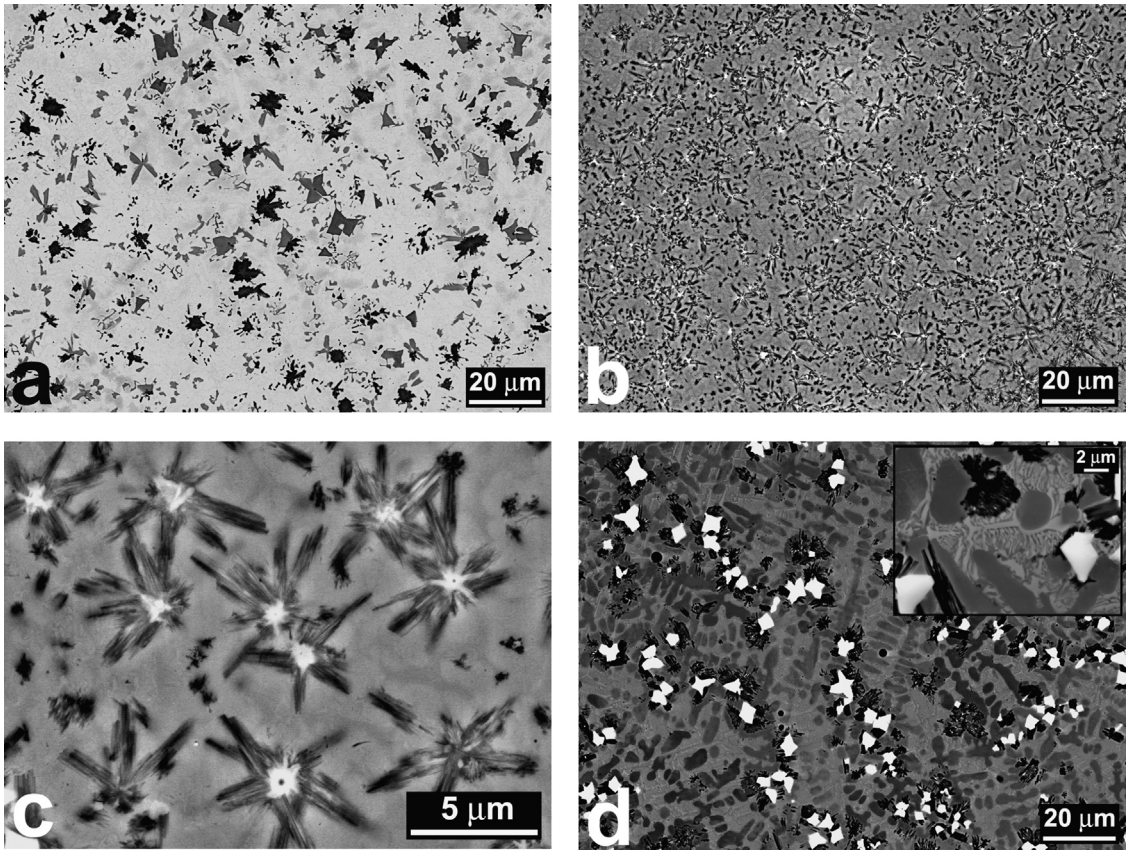

Fig. 1. SEM-BSE images comparing the microstructure of (a) Colmonoy 69 with (b) Colmonoy 69 plus 4 wt% Nb. In (c), details of the refined microstructure in (b) are shown. In (d) coarse microstructure of the deposits with 9 wt% of Nb is presented. The inset in (d) reveals details of the interdendritic region.

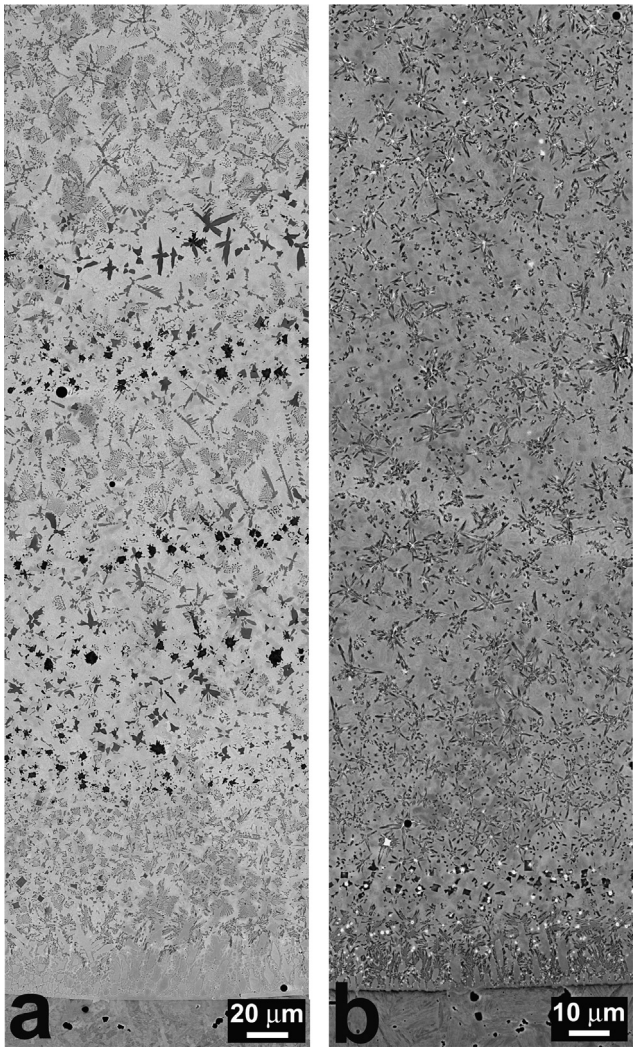

Fig. 2. (a) Heterogeneous microstructure along the depth of coating deposited from the original alloy, (b) homogenous microstructure of coatings modified by 4 wt% Nb (both image are SEM-BSE).

follow various solidification paths at different cooling rates [27]. As a result, laser-deposited Colmonoy 69 coatings have a heterogeneous microstructure as shown in Fig. 2(a) with inconsistent properties. For instance, their hardness may vary in the range of 650–950 HV [27]. Such an issue was not found in Nb-modified deposits and their microstructure was generally homogeneous as shown in Fig. 2(b). The different microstructure close to the interface in Fig. 2(a) and (b) is caused by iron concentration as a result of dilution from steel substrate. The formation mechanism for this interface layer is explained elsewhere [25].

3.2. Identification of the constituent phases

To identify the constituent phases, composition and crystallography of the intended features were determined by EDS and EBSD respectively. First, EDS spot analysis was performed to determine the composition and making a list of possible candidate phases. Later, type of the phases was conclusively determined by obtaining and indexing electron backscatter diffraction patterns. In this work, the EDS/EBSD combination was preferred over the commonly used conventional X-ray Diffraction (XRD) because of various reasons including the possibility of phase identification on phases or areas of interest (on a micrometer scale), analysis of microstructural heterogeneities in the samples, identification of phases with limited quantities, etc. For more details reference is made to [15]. A complication in the XRD phase identification is that the diffraction patterns of different phases may superimpose and consequently cause uncertainties as to which diffraction peak belongs to which phase (or phases). Although, a diffraction pattern is "unique", at least in principle, in practice there may be considerable similarities between patterns. This can obscure the identification process particularly in the case of multiphase specimens. Mixtures of phases with low symmetry, as in the case of Ni–Cr–B–Si–C coatings, are usually more difficult to differentiate due to the larger number of diffraction peaks [28]. For laser deposited coatings, extended solubility, strong texture and internal stresses in the clad layer make the XRD phase identification even less reliable [29].

Fig. 3(a) shows the SEM-BSE image of a typical feature from the Nb-modified coatings with the rod-shape phases forming on a central precipitate. Based on the previous phase identification of Colmonoy 69 deposits [15], the rods with dark contrast were expected to be Cr boride. Hence, the focus of the phase identification was on the Nb-rich precipitates. EDS spectra was obtained from the Nb-rich precipitate of Fig. 3(a) under an acceleration voltage of 5 kV to increase the accuracy for characterization of light elements such as B and C [15,25]. A challenge in identification of the EDS peaks obtained from the Nb-rich precipitate (to determine whether it was a carbide or a boride) was that the M-line for Nb (at 0.171 keV) was very close to the only peak for B, i.e. B–K (at 0.188 keV) [30]. Halographic peak deconvolution (HPD) function in the EDAX Genesis® software was used to compare the model spectra with the experimental ones as shown in Fig. 3(b). The HPD profiles including only B–K, Nb–M or both of them were superimposed on the experimental EDS spectra which all were the same. But as the L-lines for Nb (between 0.190 and 2.69 keV) were present in the spectra, the peak with the lowest energy had to contain Nb–M, either with or without B–K. This means that it was not possible to conclusively determine by EDS whether B was present in this phase or not. The same problem arose in compositional analysis of the eutectic areas as will be explained shortly. Quantification of the EDS spectra from the Nb-rich phase (Fig. 3(c)) was done by assigning both Nb and B to the lowest peak, using a standardless element coefficient (SEC) factor of 2 for C [15] and selecting the Nb-L line for quantification. The result showed that the central precipitate in Fig. 3(a) did not contain B and mostly consisted of Nb and C with almost equal quantities. As a result, the Nb-rich precipitate was expected to be of NbC type as confirmed later by EBSD results. In this work, the EDS data, including the quantitative analysis, are used mostly to determine the *possible* type of the phases. The definitive type of the intended phases will be subsequently determined using EBSD.

The EDS maps of Fig. 4 represent the distribution of different elements in the microstructure of the Nb-modified coatings. The Nb carbide precipitate was surrounded by Cr-rich rods (most probably Cr borides). The matrix consisted of Ni solid solution dendrites with Ni–Nb–Si eutectic structures. The presence of Nb in the rod-shape phases and the interdendritic regions was assessed by performing spot analysis on several locations in those phases and checking if the Nb-L lines were available. Hence, the Nb-map of Fig. 4(d) is reliable. However, as explained above, it was not possible to conclusively recognize B in areas with Nb content. For example, it was not possible to determine whether B existed in the eutectic regions or not.

Fig. 5(a) shows the SEM-BSE image of a few Nb carbide precipitates surrounded by Cr boride rods. The electron backscatter diffraction pattern from the Nb carbides could be precisely indexed as NbC as shown in Fig. 5(b) and (c). The map in Fig. 5 (d) is a combination of phase and image quality maps and shows how CrB rods formed on NbC and the colonies were surrounded by Ni-dendrites. In the map of Fig. 5(d), it seems that the interdendritic

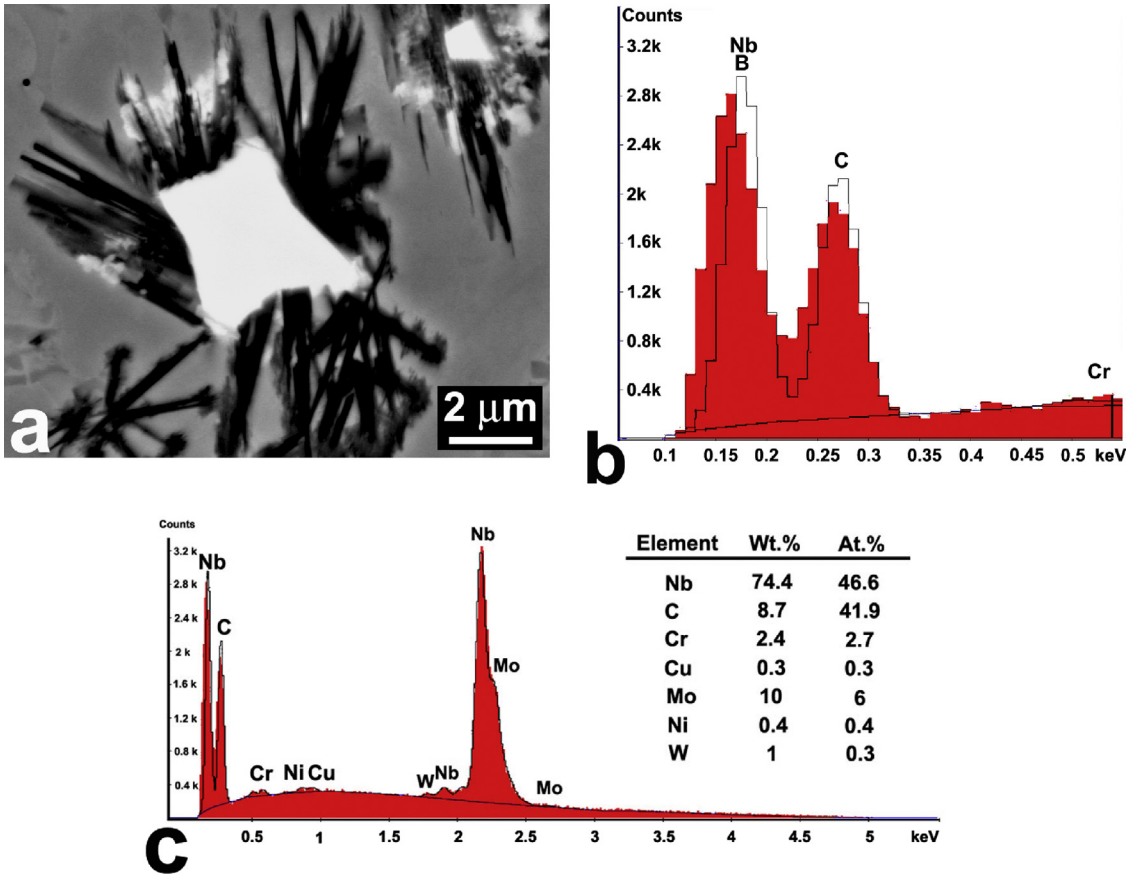

Fig. 3. (a). A large Nb-rich precipitate on which Cr boride rods have formed. (b) Part of the EDS spectrum obtained from the Nb-rich phase. The K-line for B and M-line for Nb could not be resolved using the HPD function. (c) EDS spectrum for the Nb-rich phase including percentages of its constituent elements.

areas consist of NbC which is actually not true. The interdendritic areas contain Ni plus other phases (Ni–Si–Nb type according to the EDS maps). The submicron scale of the layers in the interdendritic eutectic structure means that the electron backscatter diffraction pattern could come from more than one phase at any time. This resulted in low quality patterns which had a Ni component in most cases. As the crystal structure of Ni and NbC are identical (Cubic, O_h m3m symmetry point group) and their lattice parameters are not substantially different (0.356 nm for Ni and 0.447 nm for NbC), they can be misindexed as one another. In areas with a high quality diffraction pattern, i.e. when the signal came from either NbC or Ni dendrites, it was possible to reliably distinguish them by limiting the number of indexed bands of the diffraction pattern to 10. In each case, the EDS data provided further proof for checking the reliability of pattern indexing. In eutectic areas, diffuse Ni patterns were misindexed as NbC but with a lower image quality, i.e. darker contrast in the image quality map as shown in Fig. 5(d).

3.3. Variations of hardness and cracking tendency

As explained in Section 1, Ni–Cr–B–Si–C alloys are intended for wear applications. Consequently, refinement of their microstructure ideally should be done without deteriorating their high hardness. It can be seen in Fig. 6(a) that by addition of Nb, this goal was largely reached as the microstructural refinement shown in Fig. 1 (b) was obtained at almost the same level of hardness as the original composition [27]. An interesting characteristic of the hardness graph of Fig. 6(a) is that hardness of the deposits with different Nb additions are more or less the same. This may seem strange at first because Nb added NbC precipitates to the microstructure which have a hardness of around 2000 HV [31]. So, hardness of the coatings should normally increase for higher Nb additions. Nevertheless, the important contribution of the eutectic structure to overall hardness of Ni–Cr–B–Si–C alloys should not be ignored. The eutectic structure of Ni–Cr–B–Si–C alloys with the ratio of Si/B less than around 3 mostly consists of Ni-Ni_3B [15,32] which has a hardness of almost 1100 HV [27]. Addition of Nb not only produced hard NbC precipitates, but also modified the constitution of the eutectic structure. EDS maps of Fig. 4 showed that the interdendritic eutectics of Nb-modified coatings were rich in Ni and Si and contained some Nb. Hardness of the eutectic areas in Nb-modified coatings was in the range of 800–900 HV. This means that a possible increase in hardness because of additional NbC could be compensated by a reduction in hardness of the eutectic phases. Hence, the overall hardness remained mostly unchanged. In the previous compositional modifications of Ni–Cr–B–Si–C alloys, both increase (with Ta addition [12]) and decrease (with Ti [11] or V [7,10] additions) in the hardness of original alloys were reported. These different reports could be probably explained by the way Ta, Ti or V influenced the eutectic reactions. Otherwise, Ta, Ti or V all produce very hard carbide and boride precipitates which should normally increase the hardness.

As the hardness remained unchanged by Nb-addition and was comparable for deposits with and without Nb, changes in cracking susceptibility of the samples could be attributed to their microstructures. Fig. 6(b) shows the effect of Nb addition on cracking tendency of the samples deposited on 500 °C preheated bars. It can be seen that the cracking susceptibility of the microstructurally-refined deposits, i.e. those with around 4 wt% of Nb, was basically the same as that of deposits made from the original composition. Addition of more Nb even increased the cracking rate because excessive Nb only added

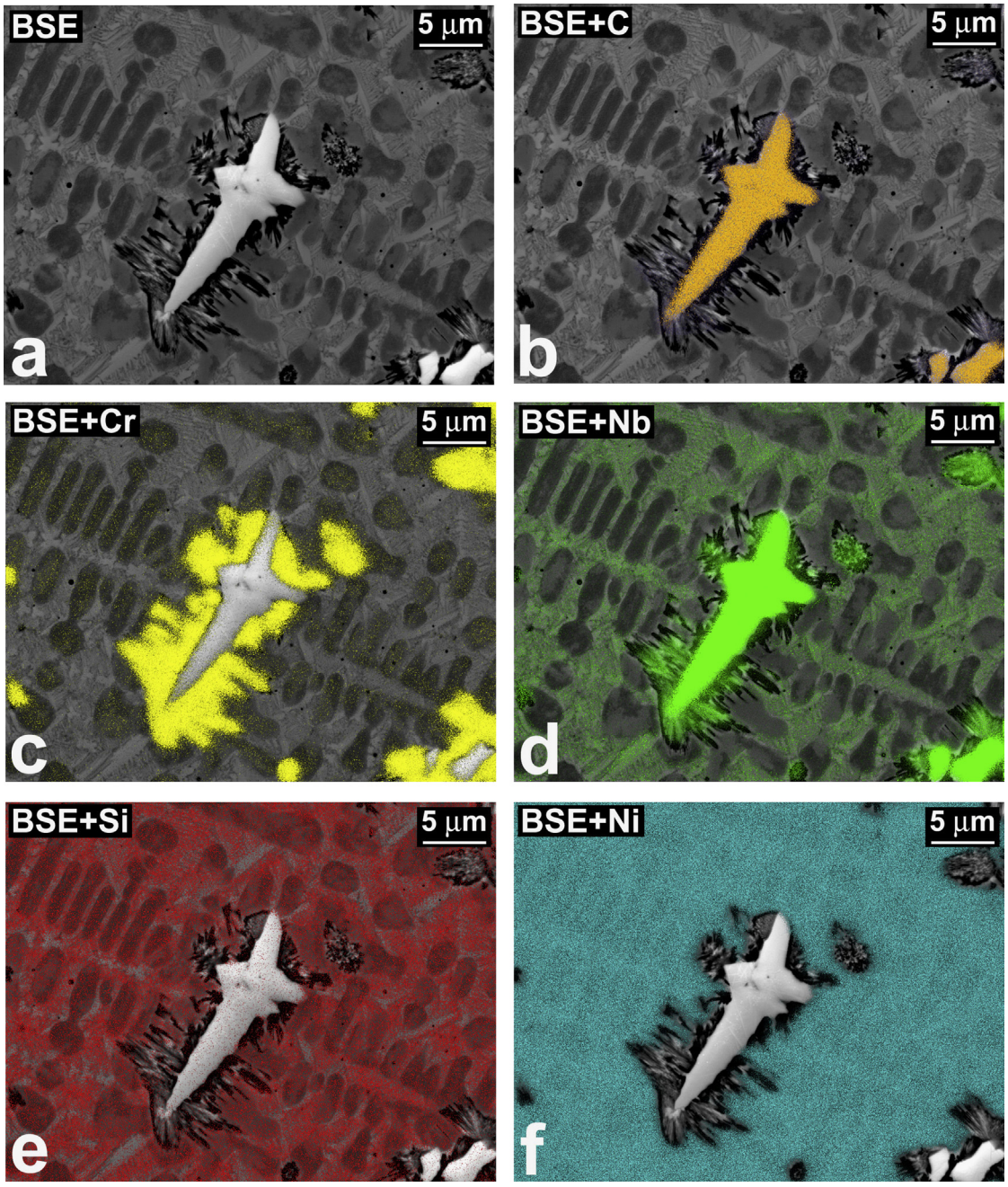

Fig.4. (a) SEM-BSE image showing a Nb-rich precipitate in its surrounding matrix and (b)–(f) EDS maps for different elements superimposed on the BSE image shown in (a).

larger and more numerous NbC precipitates and expanded the eutectic network (both brittle components) as will be discussed later.

In this study, the cracking susceptibility of the deposits was evaluated by measuring the cracking rate of multi-track coatings, i.e. the number of transversal cracks per unit area of the deposits. It is well-known for laser-clad coatings that the cracking tendency of the coatings depends not only on the intrinsic properties of the coating material such as toughness of the alloy, but also on extrinsic properties of the deposit including thickness, area, defects e.g. pores, deposition rate and temperature of the substrate among others [33]. Consequently, assessing the cracking tendency of the coating materials based on counting the number of cracks will be meaningful only under very similar extrinsic conditions and hence will have a very limited scope.

To overcome such a limitation, an attempt was made to measure the fracture toughness of laser deposited Colmonoy 69 coatings using Palmqvist indentation technique. This technique is based on indentation by a Vickers diamond pyramid indenter under known loads which are higher than some threshold necessary to generate cracks [19]. If the material is relatively hard and brittle, cracks will be generated at four corners of the indents. The fracture toughness could then be measured using the following equation [19]:

$$K_{IC} = \left(\frac{1}{3(1-\upsilon^2)\sqrt{\pi}\sqrt[3]{\sqrt{2}\pi \tan \psi}} \right) \sqrt{H}\sqrt{\frac{P}{4a}} \quad (2)$$

where υ is Poisson's ratio, ψ is the half-angle of Vickers indenter (68°), H is the hardness, P the applied load and $4a$ the total linear crack length. This technique has been previously used to measure the fracture toughness of several metallic and composite materials

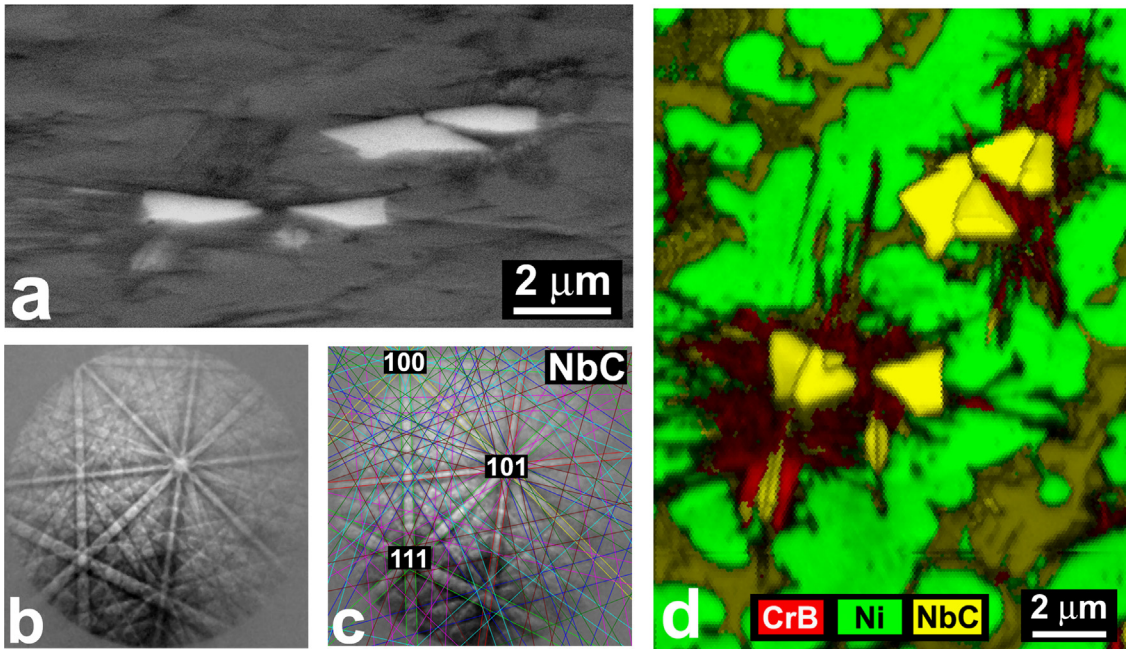

Fig. 5. (a) BSE image (70° tilted) of Nb carbides surrounded by Cr boride rods, (b) and (c) electron backscatter diffraction pattern obtained from Nb carbides which could be indexed as NbC, (d) phase map superimposed on the image quality map for the area shown in (a).

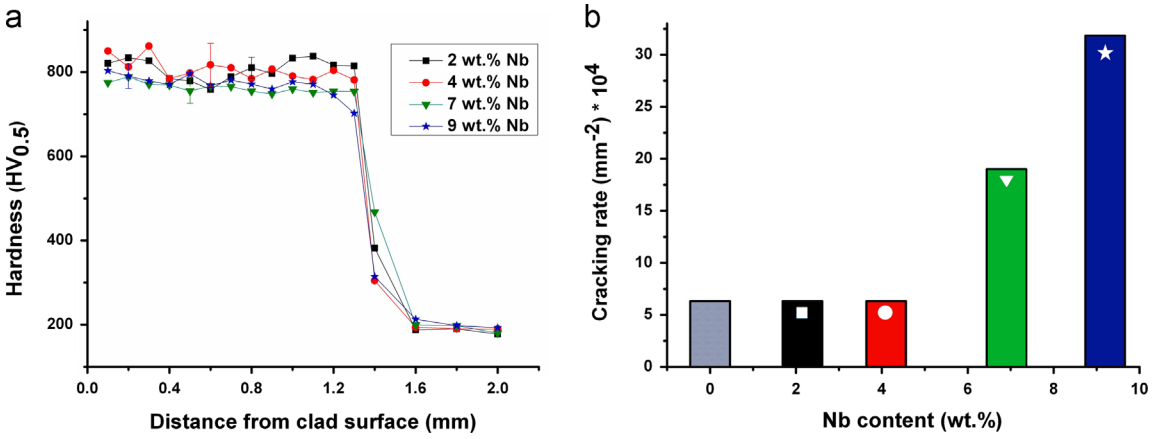

Fig. 6. Variations of (a) hardness and (b) cracking rate as a function of Nb content. The colors and markers in (b) refer to the respective hardness curve in the graph of (a).

such as W–Co [34], borided steel [35] and plasma transferred arc (PTA) welded Fe-based hardfacing alloys [19].

The idea behind indentation test for our samples was to measure the toughness of Colmonoy 69 deposits on a local scale, i.e. on an intended track. Such a local measurement was needed because of variations in microstructure of Colmonoy 69 deposits as explained before [15]. To perform the test, first the upper limit of the indentation load was found as described previously [19] to be around 1500 N and several indentations were made on tracks (at transversal cross-sections) with different microstructures using lower forces. Indentations made at a force of 125 N did not generate any corner cracks and those made at loads of 250 and 500 N contained very small corner cracks. However, massive and sudden cracks were generated at a load of 1000 N or higher for all microstructures. In the end, it was not possible to obtain a sufficient number of acceptable indents for a reliable measurement of fracture toughness as most of the indents had to be rejected because of proximity to clad–substrate interface and clad surface or closeness to defects such as pores and cracks. Fig. 7 shows an example of a rejected indent in which effects of the substrate and the diluted layer depicted as a plastic deformation

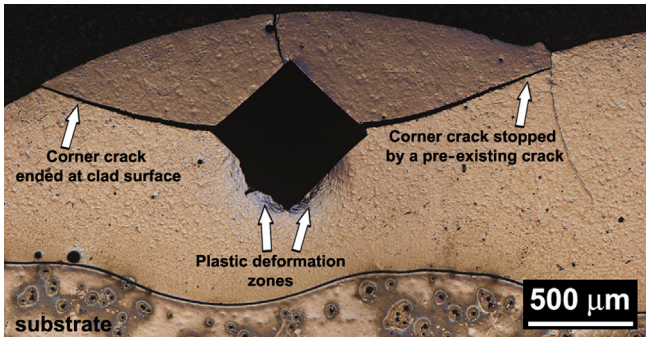

Fig. 7. An example of indentations made on the transversal cross section of a track from Colmonoy 69 coatings. This indentation was rejected because of the influence from ductile substrate, clad surface and preexisting cracks.

crack-free zone around the lower part of the indent as well as the corner cracks reaching clad surface or being stopped by cracks produced during deposition are visible.

The conclusion is that much thicker deposits are needed for such measurements. In addition, indentations should be made on

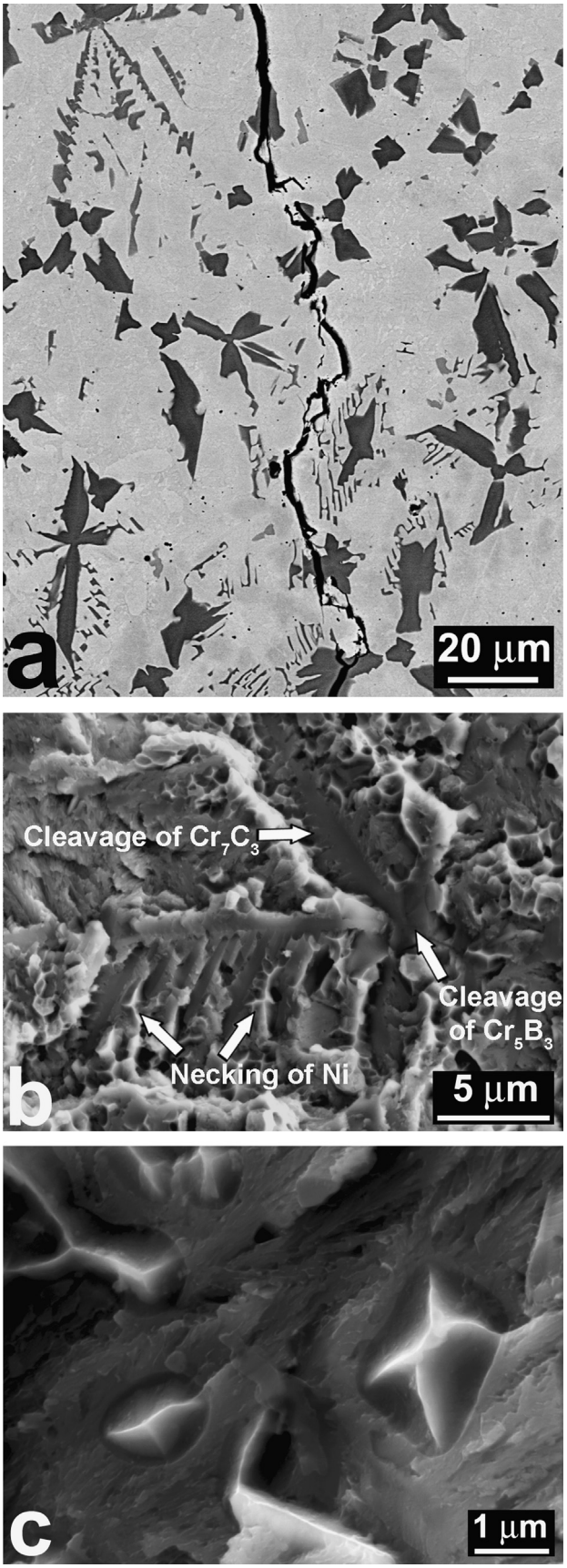

Fig. 8. (a) SEM-BSE image showing an example of crack growth path in Colmonoy 69 coatings. The cracks apparently follow the precipitates (dark phases). (b) Fracture surface of Colmonoy 69 coatings showing different fracture modes for Ni- and Cr-rich precipitates. (c) Fracture surface showing ductile failure of Ni in comparison to the quasi-cleavage fracture of the interdendritic eutectics.

the top surface of the polished clad layers and not on their cross-section (which was not possible to do for Colmonoy 69 deposits because of microstructural variations). Ultimately, the cracking rate was used to evaluate the cracking susceptibility of alloy with and without Nb. Given the similar set of extrinsic characteristics of the clad layers (constant size, geometry and type of the substrate, similar heating and cooling conditions, similar clad thickness and length and the same deposition rate), counting the number of cracks per unit clad area could be regarded as a meaningful measure to compare cracking propensity of the coating alloys.

3.4. Analysis of the crack growth paths

The crack growth paths in Colmonoy 69 and Nb-modified Colmonoy 69 were studied by SEM and OM to understand the microstructural aspects of cracking phenomena. SEM-BSE images of the crack propagation path such as the one presented in Fig. 8(a) suggested that the main contributors to crack growth in Ni–Cr–B–Si–C deposits are the Cr-rich precipitates as also reported by previous researchers [7,14]. However, the role of the other two groups of constituent phases, i.e. eutectics and Ni dendrites could not be deduced from the BSE image because Ni and constituents of the eutectic structures could not be properly distinguished by BSE imaging [15].

The fracture modes of Cr-rich precipitates, eutectics and Ni dendrites were assessed by observing the fracture surfaces of Colmonoy 69 deposits. To obtain the fracture surfaces, single tracks of Colmonoy 69 were deposited with zero dilution. Some of the tracks were detached and fractured during deposition. In Fig. 8(b), the cleavage fracture of Cr_5B_3 and Cr_7C_3 precipitates and the ductile fracture of Ni with clear neck formation are noticeable. Type of the constituent phases is recognized based on their morphologies as characterized previously [15]. Fig. 8(c) shows an area of the fracture surface consisting of Ni grains and interdendritic eutectic network. While the ductile behavior of Ni grains and their considerable plasticity are depicted by multiple necks, the eutectic network did not show much plasticity and fractured in a quasi-cleavage mode. These observations suggest that the eutectic structure in Colmonoy 69 deposits should have contributed to crack growth and clearly Ni was the only ductile component of the system.

Observations of the crack propagation path using OM revealed other details. Fig. 9(a) shows the OM image of crack growth in the same area as in Fig. 8(a). While the BSE image could not explain the tortuous crack path, the OM image in Fig. 9(a) clearly shows how cracks propagate not only in the Cr-rich precipitates, but also through the eutectic network (visible as a brown matrix). In addition, the OM image of Fig. 9(a) reveals the role of Ni dendrites (bright areas) in deflecting the cracks and forcing them to bridge.

As OM proved to be more capable of revealing the true nature of crack propagation, crack growth path in the refined microstructure of Nb-modified deposit was observed using OM as shown in Fig. 9(b). The Cr borides in the microstructure shown in Fig. 9(b) are much smaller and are not anymore a major contributor to crack propagation. However, similar to Colmonoy 69 deposits, the continuous network of eutectic phases still provided the easy route for cracks to propagate. These observations confirm the pivotal role of the network of hard eutectic phases in cracking of the deposits from these alloys.

3.5. Microstructural observation using optical microscopy

Microstructure of the coatings with different amount of Nb was reexamined by OM as optical microscopy proved to be a useful tool for microstructural analysis of these alloys, especially to study the crack growth paths as shown above. Fig. 10 presents the OM microstructural images of deposits with 4 and 9 wt% of Nb. The differences between scale of the constituent phases and quantity

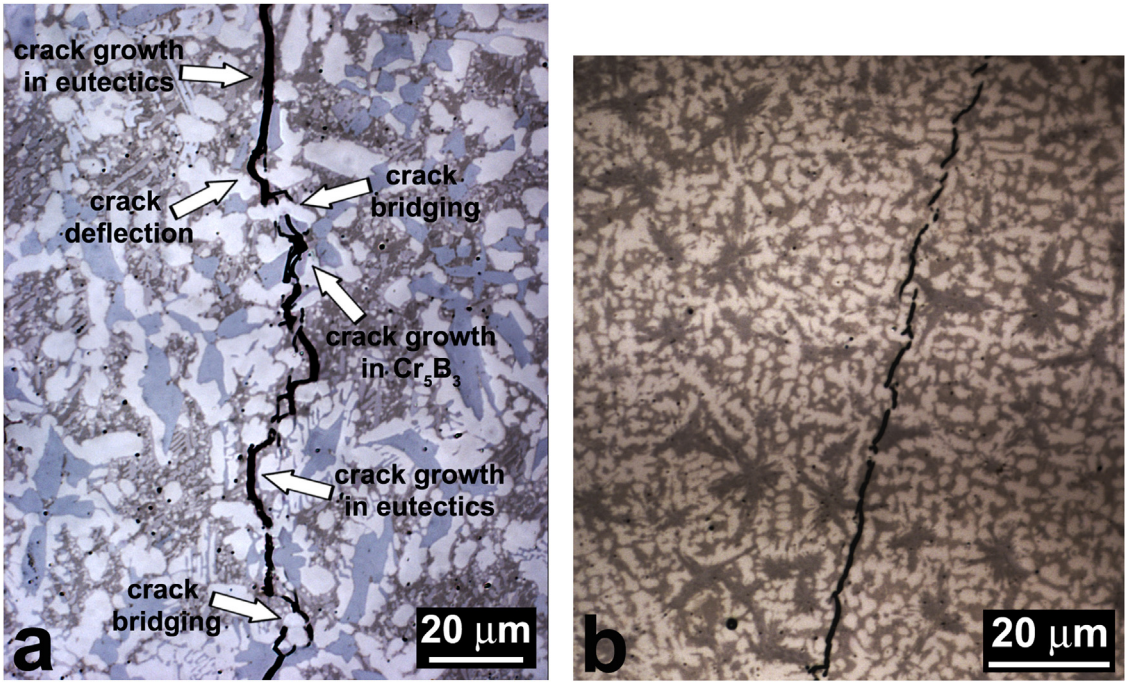

Fig. 9. (a) OM image of the area shown in Fig. 8(a) in which much more details about the crack growth path are visible as indicated by arrows and (b) crack growth in the refined microstructure of Nb-modified deposits.

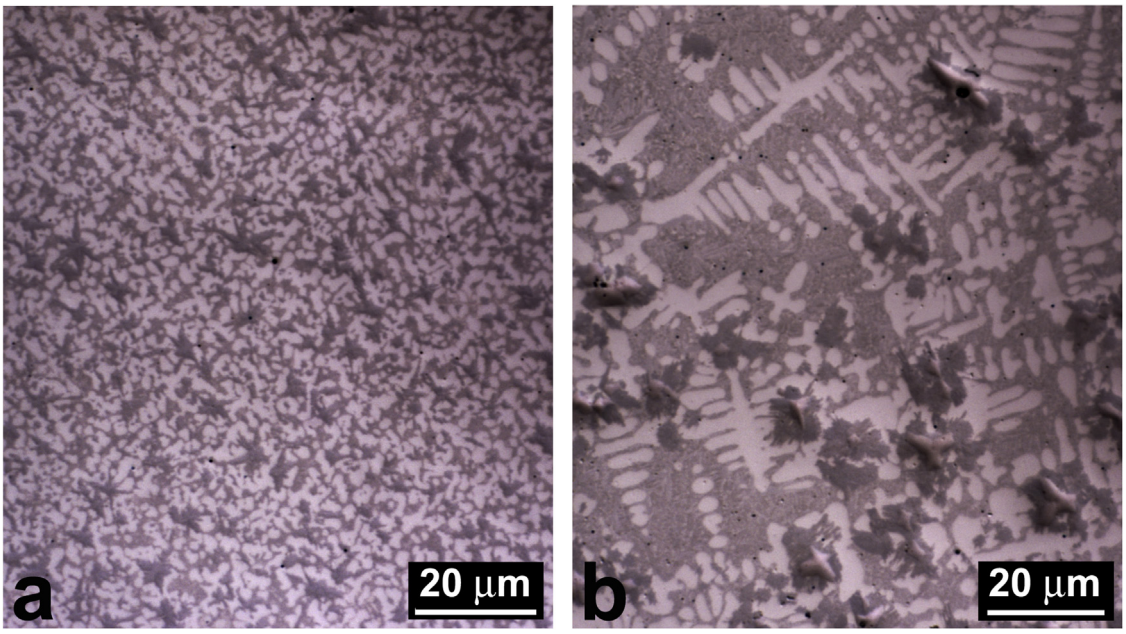

Fig. 10. OM microstructural images from coatings modified by (a) 4 wt% and (b) 9 wt% of Nb.

of the interdendritic eutectic are obvious. In comparison to SEM micrographs (both SE and BSE), OM images give a better overview of the microstructure in these alloys and are especially helpful to observe their eutectic structure. The OM images of Fig. 10 also clarify the explanations given in Section 3.3 about the effects of Nb content on hardness of the coatings.

4. Discussion

Addition of Nb in specific quantities was shown to induce a true microstructural refinement in the original Ni–Cr–B–Si–C alloy (Colmonoy 69) without deteriorating its hardness. Nb fulfilled the requirements of forming a phase at high temperatures with little solubility in Cr-rich phases which could act as nucleation agents for them [10]. NbC precipitates provided nucleation sites for CrB rods and this substantially refined the microstructure. In addition, microstructural sensitivity of the original composition to variations of solidification conditions subsided by addition of Nb. As a result, no considerable microstructural heterogeneities could be found in the Nb-modified coatings.

From the above-mentioned perspectives, Nb could be regarded as a useful alloying addition for the high-alloy grades of Ni–Cr–B–Si–C family. However, Nb addition and the subsequent refinement of hard Cr-rich precipitates did not fulfill the expectations for enhancement of the coatings' fracture toughness. The outcome

was not in line with the findings of a previous research on the correlation between structural scale of the strengthening components and fracture toughness of wear-resistant alloys in which the authors hypothesized that "the reduction of the structural scale of the microstructure would enhance the fracture toughness" [18]. In [18], it was shown that microstructural refinement of Fe-base wear resistant alloy deposits could enhance their fracture toughness while preserving hardness of the deposits. In this way, the so-called "hardness–toughness paradox" could be solved by preserving the quantity of hard components but reducing their scale. Although a similar phenomenon could be induced in the laser deposited Ni–Cr–B–Si–C alloys, i.e. microstructural refinement while preserving the level of hardness, the outcome was not consistent with the above-mentioned general hypothesis.

This discrepancy could be explained based on the different phase constitution and microstructure of the laser deposited Ni–Cr–B–Si–C alloys. If the microstructure of the alloy consists of strengthening components in a continuous matrix of ductile phase as in [18], then refinement of the strengthening components may enhance the fracture toughness. This is so because the ductile phase may effectively isolate cracks in the hard components by providing plastic zones ahead of the cracks. In laser deposited Ni–Cr–B–Si–C alloys such as Colmonoy 69 or Nb-modified Colmonoy 69, although carbide and boride precipitates were engulfed by Ni dendrites as shown in Fig. 5(d), a continuous network of eutectic structure filled the spaces between Ni dendrite arms.

Analysis of the crack growth paths and fracture surfaces of the samples showed that besides Cr-rich precipitates, the eutectic network also played an important role in the cracking process. In fact, as it can be seen in Fig. 10, cracks propagated mostly through the continuous network of eutectics. This happened because the eutectic structure in Ni–Cr–B–Si–C alloys with the ratio of Si/B less than 3 (Si/B for Colmonoy 69:1.33) mostly consists of Ni–Ni_3B [15] which is very hard and brittle [27]. Fig. 8(c) clearly shows the large difference in plasticity between the eutectic structure and the ductile Ni grains. Although the eutectic network also contains lamella of ductile Ni, these lamellae are too thin to have any significant effect on the toughness. The eutectic phases in the Nb-modified system were not as hard as those of the original alloy. However, still they formed an interconnected network which could actively contribute to crack propagation in the refined microstructure as shown in Fig. 10(b).

In the comprehensive work on the fracture mechanism and toughening of plasma transferred arc (PTA) deposited Ni–Cr–B–Si–C alloys, Cockeram [13] concluded that crack bridging mechanism, i.e. necking and plastic elongation of the Ni dendrites can explain the fracture behavior of Ni–Cr–B–Si–C alloys. Fig. 10(a) confirms that Ni dendrites effectively deflect the propagating cracks and force them to bridge frequently which is in line with the findings of Cockerham. Toughening of a brittle matrix by crack bridging (ΔK_{CB}) can be described as [13,36]

$$\Delta K_{CB} = C.E_d\left[V_f\sigma_o/E_d a_o\right]^{0.5} \quad (3)$$

where C is a material-related constant, E_d, V_f, σ_o and a_o are the elastic modulus, volume fraction, yield stress and radius of the ductile phase (Ni dendrites) respectively. Measurement of the fracture toughness values for PTA welded Ni–Cr–B–Si–C samples showed that in (3), V_f and a_o are the main parameters affecting the amount of the crack bridging in these alloys [13]. This means that increasing the toughness of Ni–Cr–B–Si–C alloys requires higher percentages and/or coarser Ni dendrites. The phase formation behavior of Ni–Cr–B–Si–C alloys happens in such a way that increasing the percentage of Ni dendrites will inevitably decrease the fraction of the Ni–B–Si eutectics and hence reduce the overall hardness of the deposits [27]. In addition, laser deposited samples usually have very fine Ni dendrites as a result of their rapid solidification. Consequently, enhancing the crack bridging phenomena to toughen the Ni–Cr–B–Si–C laser deposited coatings while preserving their high hardness will be inherently difficult.

In the Ni–Cr–B–Si–C alloy system, a sole microstructural refinement of the precipitates cannot be a viable toughening mechanism because although the ductile phase may deflect the cracks propagating to and from the precipitates, it cannot prevent them to use the continuous eutectic network as an easy growth path. Consequently, an effective toughening of these alloys will not happen unless the eutectic network is changed in type or its continuity is disrupted. Such changes may require new alloying additions to the existing Ni–Cr–B–Si–C alloys and changing the content of alloying elements to induce eutectic reactions other than the current ones. The Nb-modified system discussed in this work can act as a base for further alloy developments in which the focus could be on modification of the eutectic structure.

5. Conclusions

Nb addition in suitable quantities could substantially refine the microstructure of laser deposited Ni–Cr–B–Si–C alloy coatings by producing submicron NbC precipitates which acted as nucleation sites for CrB rods. Hardness of the Nb-modified coatings was around 800 HV which is almost the same as that of the original alloy. However, contrary to the expectations, microstructural refinement did not decrease cracking tendency of the Nb-modified coatings. The reason for this failure was that not only the hard precipitates, but also the continuous network of hard eutectic phases contributed to the cracking process. This means that toughening of Ni–Cr–B–Si–C alloys could not be reached solely by reduction in structural scale of the hard precipitates. But modifying the type of constituent phases in the eutectic structure or disruption of their continuous network is also needed to obtain high hardness–high toughness Ni-base hardfacing alloys.

Acknowledgments

This research was carried out under project number MC7.06259 in the framework of the Research Program of the Materials innovation institute M2i (www.m2i.nl). The Wall Colmonoy Ltd. (The UK) is acknowledged for providing Colmonoy 69 powder.

References

[1] A. Conde, F. Zubiri, y J. de Damborenea, Mater. Sci. Eng. A 334 (2002) 233.
[2] J.M. Miguel, J.M. Guilemany, S. Vizcaino, Tribol. Int. 36 (2003) 181.
[3] E. Fernández, M. Cadenas, R. González, C. Navas, R. Fernández, J. Damborenea, Wear 259 (2005) 870.
[4] Song Jianli, Li Yongtang, Fu Jianhua, Deng Qilin, Hu Dejin, in: Proceedings of International Technology and Innovation Conference (ITIC), IET, 2009, pp. 68–72.
[5] C.P. Paul, A. Jain, P. Ganesh, J. Negi, A.K. Nath, Opt. Lasers Eng. 44 (2006) 1096.
[6] A. Angelastro, S.L. Campanelli, A.D. Ludovico, Adv. Mater. Res. 83–86 (2009) 842.
[7] D. Wang, E. Liang, M. Chao, B. Yuan, Surf. Coat. Technol. 202 (2008) 1371.
[8] S. Zhou, X. Dai, H. Zheng, Opt. Laser Technol. 43 (2011) 613.
[9] Y. Huang, X. Zeng, Appl. Surf. Sci. 256 (2010) 5985.
[10] I. Hemmati, J.C. Rao, V. Ocelík, J.T.M. Hosson, J. Mater. Sci. 48 (2013) 3315.
[11] M.-J. Chao, E.-J. Liang, Surf. Coat. Technol. 179 (2004) 265.
[12] T. Yu, Q. Deng, G. Dong, J. Yang, Appl. Surf. Sci. 257 (2011) 5098.
[13] B.V. Cockeram, Metall. Mater. Trans. A: Phys. Metall. Mater. Sci. 33 (2002) 33.
[14] T. Yu, Q.-L. Deng, W. Zhang, G. Dong, J. Yang, J. Shanghai Jiaotong Univ. (Sci.) 46 (2012) 1043.
[15] I. Hemmati, J.C. Rao, V. Ocelík, J.T.M. De Hosson, Microsc. Microanal. 19 (2013) 120.
[16] R. Jendrzejewski, I. Kreja, G. Śliwiński, Mater. Sci. Eng. A 379 (2004) 313.
[17] W.D. Callister, Materials Science and Engineering: An Introduction, 7th ed, John Wiley & Sons, New York, 2007.
[18] D.J. Branagan, M.C. Marshall, B.E. Meacham, Mater. Sci. Eng. A 428 (2006) 116.

[19] B.E. Meacham, M.C. Marshall, D.J. Branagan, Metall. Mater. Trans. A 37 (2006) 3617.
[20] I. Barin, Thermochemical Data of Pure Substances, 3rd ed., VCH, Weinheim, New York, 1995.
[21] T.F. Fedorov, N.M. Popova, L.V. Gorshkova, R.V. Skolozdra, Y.B. Kuz'ma, Sov. Powder Metall. Metal Ceram. 7 (1968) 193.
[22] L.A.B. Júnior, G.C. Coelho, C.A. Nunes, P.A. Suzuki, J. Phase Equilibria 24 (2003) 140.
[23] H.W. Hugosson, U. Jansson, B. Johansson, O. Eriksson, Chem. Phys. Lett. 333 (2001) 444.
[24] E. Toyserkani, Laser Cladding, CRC Press, Boca Raton, FL, 2005.
[25] I. Hemmati, V. Ocelík, J.T.M. De Hosson, Mater. Lett. 84 (2012) 69.
[26] T.G. Woodcock, O. Gutfleisch, Acta Mater. 59 (2011) 1026.
[27] I. Hemmati, V. Ocelík, J.T.M. De Hosson, in: Surface Effects and Contact Mechanics X, Eds. J.Th.M. De Hosson and C.A. Brebbia, WIT Transactions on Engineering Sciences. WIT Press, 71 (2011) 287–296, http://dx.doi.org/10.2495/SECM110251.
[28] B.D. Cullity, S.R. Stock, Elements of X-Ray Diffraction, 3rd ed., Prentice Hall, 2001.
[29] Q. Li, D. Zhang, T. Lei, C. Chen, W. Chen, Surf. Coat. Technol. 137 (2001) 122.
[30] G. Zschornack, Handbook of X-ray Data, Springer, New York, 2006.
[31] J.J. Gilman, Chemistry and Physics of Mechanical Hardness, Wiley, Hoboken, NJ, 2009.
[32] K. Tanaka, Hardfacing Ni-base Alloys, U.S. Patent 4,404,049, 1983.
[33] F. Wang, H. Mao, D. Zhang, X. Zhao, Y. Shen, Appl. Surf. Sci. 255 (2008) 3267.
[34] R. Spiegler, S. Schmadder, L. Sigl, J. Hard Mater. 1 (1990) 147.
[35] I. Campos, R. Rosas, U. Figueroa, C. VillaVelázquez, A. Meneses, A. Guevara, Mater. Sci. Eng. A 488 (2008) 562.
[36] M.F. Ashby, F.J. Blunt, M. Bannister, Acta Metall. 37 (1989) 1847.